Acknowledgment

The present work was supported by the National Research Laboratory Program (M1-0203-00-0006) of the Ministry of Science and Technology, Republic of Korea. The authors fully appreciate the financial support.

References

[1]Brüege, U., and Görlach, T., "Solution for the Geostationary Collocation Problem," AIAA Paper 93-3789, 1993.

[2]Carlini, S., and Graziani, F., "An Eccentricity Control Strategy for Coordinate Station Keeping," *Proceeding of the 3rd International Symposium on Spacecraft Flight Dynamics*, SP-326, edited by J. J. Hunt, ESA, Darmstadt, Germany, 1991, pp. 17–21.

[3]Maisonbe, L., and Dejoice, C., "Analysis of Separation Strategy for Colocated Satellite," *Proceeding of the 3rd International Symposium on Spacecraft Flight Dynamics*, SP-326, edited by J. J. Hunt, ESA, Darmstadt, Germany, 1991, pp. 5–9.

[4]Lee, B. S., Lee, J. S., and Choi, K. H., "Analysis of a Stationkeeping Maneuver Strategy for Collocation of Three Geostationary Satellites," *Control Engineering Practice*, Vol. 7, July 1999, pp. 1153–1161.

[5]Lee, B. S., and Choi, K. H., "Collocation of Two GEO Satellites and One Inclined GSO Satellite," *Aerospace Science Technology*, Vol. 4, April 2000, pp. 507–515.

[6]Eckstein, M. C., "On the Separation of Collocated Geostationary Satellites," German Space Operations Center, TN87-20, Wessling, Germany, Dec. 1987.

[7]Pocha, J. J., "Stationkeeping," *An Introduction to Mission Design for Geostationary Satellites*, 1st ed., D. Reidel, Dordrecht, The Netherlands, 1987, pp. 80–129.

C. McLaughlin
Associate Editor

Dual-Code Thin-Layer Parabolized Navier–Stokes Strategy for Supersonic Flows over Spinning Bodies

Omid Abouali,* Mohammad M. Alishahi,† and Homayoon Emdad‡
Shiraz University, 71344 Shiraz, Iran
and
Goodarz Ahmadi§
Clarkson University, Potsdam, New York 13699-5725

Nomenclature

E, F, G	=	inviscid fluxes
E_v, F_v, G_v	=	viscous fluxes
$\tilde{E}, \tilde{F}, \tilde{G}$	=	fluxes in general curvilinear coordinates
J	=	Jacobian of transformation
P	=	pressure
Q	=	primitive variable matrix
q_x, q_y, q_z	=	heat-conduction terms
u, v, w	=	velocities
V	=	volume
x, y, z	=	Cartesian coordinates
α	=	angle of attack
ξ, η, ζ	=	general curvilinear coordinates
τ_{ij}	=	tensor of stresses
ρ	=	specific mass

Received 26 June 2002; revision received 3 May 2003; accepted for publication 13 May 2003.

*Assistant Professor, Department of Mechanical Engineering.
†Professor, Department of Mechanical Engineering.
‡Assistant Professor, Department of Mechanical Engineering. Member AIAA.
§Professor, Department of Mechanical and Aeronautical Engineering.

Introduction

THIS study is concerned with developing a supersonic combined computer code to be used on microcomputers as an aerodynamic design tool in preliminary and middesign stages. The CPU time needed for solving the Navier–Stokes equations for compressible flows is very high and normally requires a large computer memory; thus, in most cases supercomputers are used for such extensive computational efforts.[1,2]

In preliminary design stages, however, extensive computer resources might not be available and/or might be too costly. In practice, some approximate forms of the Navier–Stokes equations are solved.[3] The thin-layer Navier–Stokes (TLNS) equations are derived by neglecting the viscous terms in a streamwise direction. Although the use of TLNS decreases the required computer time and memory, the required resources are still large. The parabolized Navier–Stokes (PNS) equations are obtained by further neglecting the unsteady terms in the TLNS equations. For supersonic flows the PNS equations have a hyperbolic–parabolic nature and can be solved using space-marching algorithms. Therefore, the solution proceeds plane by plane, considerably decreasing the required computer resources. Using the PNS equations, however, is limited to the cases of supersonic flows with small streamwise pressure gradients and a starting plane of data is required in all cases to initiate the computation. Also, certain modeling must be taken for the subsonic streamwise pressure gradient within the boundary layer to suppress the upstream propagation of information. Hence the PNS equations are not appropriate for blunt-body and wing-body problems because of the subsonic flow restriction.

One alternative is to use a dual-code combination, that is, using the PNS code in most of the region and the use of the TLNS code wherever the PNS is not applicable. Wood and Thompson[4] implemented such a combined solution procedure for hypersonic flow fields about blunted slender bodies using a TLNS code (LAURA[5]) in the nose region and a PNS code (UPS[6–8]) in the afterbody region. The application of integrated LAURA-UPS procedure was demonstrated for two slender blunted cones.

Sturek et al.[9] reported the application of a three-dimensional TLNS solver, which was a central-differencing technique to predict the Magnus force and moments for hemispherical and flattened blunt-nose configuration and the PNS code to compute the flow over the remainder of the spinning shell. Emdad et al.[10] developed a PNS code to provide solutions on supersonic spinning slender bodies at high Reynolds numbers and moderate angles of attack. This code is a finite volume, shock-capturing, upwind scheme with the Roe method[11] that is fully implicit and second-order accurate in the crossflow planes. An option was included for turbulence using the Baldwin–Lomax model[12] and its modifications. This code is used as a part of a dual-code strategy in this study.

Alishahi et al.[13,14] developed a TLNS code. Roe's method is used to discretize the inviscid terms[15,16] and central differencing for the viscous terms. Time-derivative terms are discretized with the explicit technique. The Baldwin–Lomax model[12] and Degani–Schiff modifications are used for turbulence modeling. The algorithm is based on a finite volume approach. This code is used as the other part of the dual code.

In this study a PNS code is combined with a TLNS code to solve supersonic flows around the spinning bodies. An interpolation subprogram receives the data from the TLNS code and then prepares the needed initial data plane for PNS code. The cases of a supersonic flow over a nonspinning and spinning secant-ogive at Mach number 3 are studied. The dual-code simulation results are compared with experimental data, and the results are in good agreement with experimental data. It is found that the dual-code computer time is one order of magnitude less than that of TLNS code at comparable accuracy and thus provides a useful tool in preliminary design stages. Application of this dual-code procedure to a wing-body combination

is presently undertaken, and the results will be presented in the near future.

Model Description

In this study a TLNS code developed by Alishahi et al.[13,14] is combined with a PNS code.[10,17] This provides one of the few uses of an upwind scheme dual code for spinning bodies. As a result, the use of artificial viscous terms for accurate shock capturing that is necessary for central-differencing scheme codes was not required. This dual-code procedure is used to study nonspinning and spinning slender-body test cases. It is recognized that any real vehicle, no matter how slender the afterbody is, will have a blunted nose. Therefore, the procedure is set forward for solving flowfields with a time-marching Navier–Stokes scheme on the nose region followed by a space marching scheme on the afterbody. The cases studied are supersonic flows over a nonspinning and spinning secant-ogive with Mach 3 at incidence angle 10 deg. For the spinning case several different incidence angles and a nondimensional spin rate of 0.19 are used.

Governing Equations

Navier–Stokes equations in Cartesian coordinates in the conservative form are

$$Q_t + (E - E_v)_x + (F - F_v)_y + (G - G_v)_z = 0 \tag{1}$$

$$Q = \begin{bmatrix} e \\ \rho \\ \rho u \\ \rho v \\ \rho w \end{bmatrix} \qquad E = \begin{bmatrix} (e+p)u \\ \rho u \\ \rho u^2 + p \\ \rho uv \\ \rho uw \end{bmatrix}$$

$$F = \begin{bmatrix} (e+p)v \\ \rho u \\ \rho uv \\ \rho v^2 + p \\ \rho wv \end{bmatrix} \qquad G = \begin{bmatrix} (e+p)w \\ \rho w \\ \rho uw \\ \rho vw \\ \rho w^2 + p \end{bmatrix} \tag{2}$$

$$E_v = \begin{bmatrix} u\tau_{xx} + v\tau_{xy} + w\tau_{xz} - q_x \\ 0 \\ \tau_{xx} \\ \tau_{xy} \\ \tau_{xz} \end{bmatrix}$$

$$F_v = \begin{bmatrix} u\tau_{yx} + v\tau_{yy} + w\tau_{yz} - q_y \\ 0 \\ \tau_{yx} \\ \tau_{yy} \\ \tau_{yz} \end{bmatrix}$$

$$G_v = \begin{bmatrix} u\tau_{zx} + v\tau_{zy} + w\tau_{zz} - q_z \\ 0 \\ \tau_{zx} \\ \tau_{zy} \\ \tau_{zz} \end{bmatrix} \tag{3}$$

where e is total energy. The stress tensor components are computed by the Stokes relation.

Equation (1) can be expressed in terms of generalized curvilinear coordinates system as

$$\partial\tilde{Q}/\partial t + \partial(\tilde{E} - \tilde{E}_v)/\partial\xi + \partial(\tilde{F} - \tilde{F}_v)/\partial\eta + \partial(\tilde{G} - \tilde{G}_v)/\partial\zeta = 0 \tag{4}$$

$$\tilde{Q} = Q/J \tag{5}$$

We now apply the thin-layer approximation to the transformed Navier–Stokes equations. This approximation allows us to drop out all viscous terms containing partial derivatives with respect to ξ and ζ, where η is generally perpendicular to walls. The resulting thin-layer equations can be written as

$$\partial\tilde{Q}/\partial t + \partial\tilde{E}/\partial\xi + \partial(\tilde{F} - \tilde{F}_v)/\partial\eta + \partial\tilde{G}/\partial\zeta = 0 \tag{6}$$

and the PNS equations can be derived with dropping out the unsteady terms:

$$\partial\tilde{E}/\partial\xi + \partial(\tilde{F} - \tilde{F}_v)\partial\eta + \partial(\tilde{G} - \tilde{G}_v)/\partial\zeta = 0 \tag{7}$$

Detailed explanations were presented.[10,13,17]

Matching Process

In this study a dual-code PNS-TLNS strategy is used for solving the flowfield over bodies. In this approach the TLNS code is first used to evaluate the flowfield around the nose of the body. This will generate an initial plane for the PNS code. An interpolation subprogram is prepared for matching of the two codes. Input to this subprogram is the grid location and the field properties data from the TLNS code. The grid geometry of the initial plane of the PNS code is also imported to this subprogram. Afterward this subprogram searches for the neighborhood grids of each PNS grid point. Knowing the neighborhoods of each grid point, the field properties for the PNS grid points are linearly interpolated from the field properties extracted from the TLNS code. The interpolation process is performed for the velocity components U, V, W; density ρ; and total energy e.

Grid Generation

The grid generation is performed in two steps. In the first a few two-dimensional grids of O type are generated at different crossflow planes. In the second step for the TLNS code, these two-dimensional grids are connected to make a three-dimensional grid.

It is obvious that the PNS code needs only two plane of this O-type grid, and they are generated at the time of the streamwise marching. The outer radius of the grids is obtained using the Taylor–Makcoll solution around the nose of the ogive to include the outer shock. A crossflow plane of generated grid for a secant-ogive with incidence angle 10 deg is shown in Fig. 1. The radial distribution of the grids is adaptively controlled so that the distance of the first node from the body surface r^+ will be in the range of 5–10. The freestream boundary condition is applied on the outer boundary and the zero velocity and zero temperature gradient at the body surface.

Results

The first test case is the supersonic turbulent flows at Mach 3 around a secant-ogive at the incidence angle 10 deg. The dimension of the computational grid used for TLNS code at the nose of the ogive is $6 \times 46 \times 38$ in the longitudinal, radial, and circumferential directions. The dimension of the computational grid for the PNS

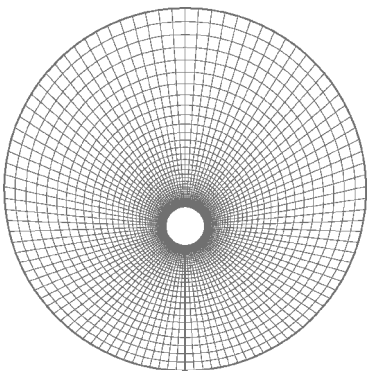

Fig. 1 Axial cross section of generated grid for a secant-ogive with incidence angle of 10 deg.

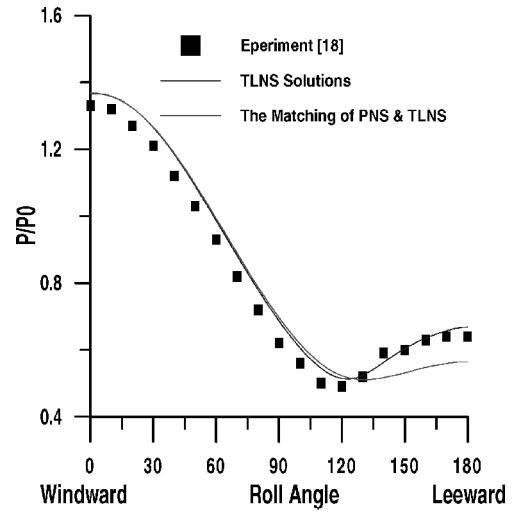

a) $x/D = 3.33$

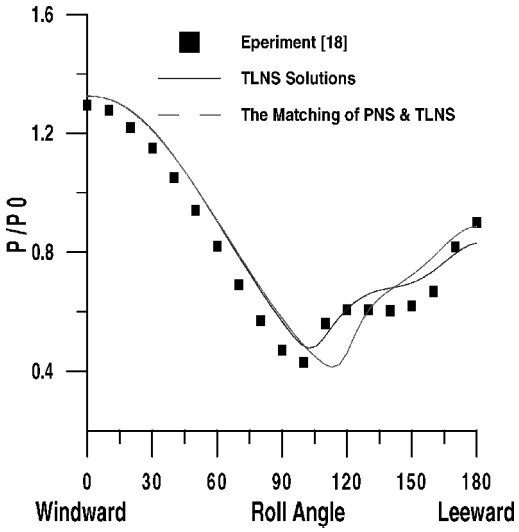

b) $x/D = 5.77$

Fig. 2 Comparison of pressure at $\alpha = 10$ and Mach number = 3.

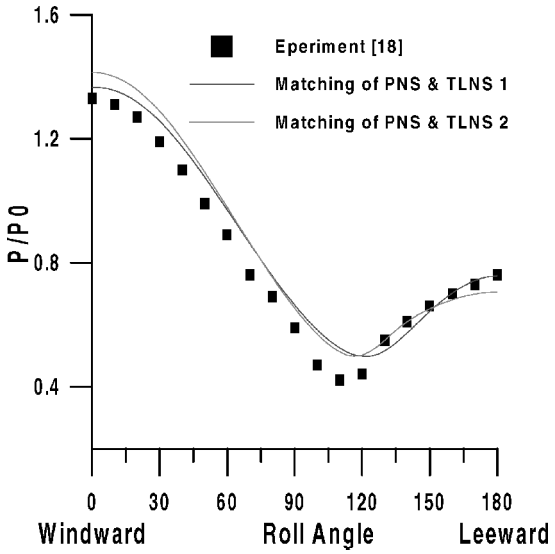

a) $x/D = 4.14$

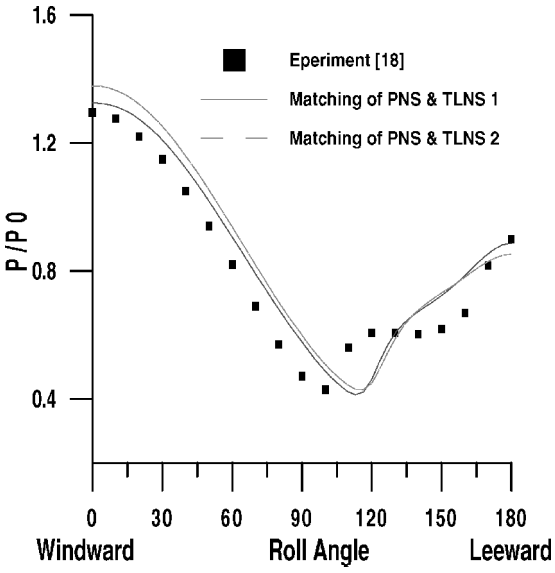

b) $x/D = 5.77$

Fig. 3 Comparison of pressure for different initial data plane at $\alpha = 10$ and Mach number = 3.

code at the afterbody of the ogive-cylinder is 52×46 in the radial and circumferential directions. In this case because of the symmetrical condition, half of the flow domain is solved.

The grid-convergence test was also performed. It was shown that using a finer grid did not show any difference in the numerical results compared with the grid size just noted.

An interpolation subprogram receives the data from the TLNS code and then prepares the needed initial data plane for PNS code. This step resolved the problem reported by Wood and Tompson[4] in requiring the exact same grids at the interface.

The circumferential pressure distribution at different axial sections for a supersonic flow with $Re_\infty = 6.4 \times 10^6$ based on model length was investigated. Figure 2 shows this comparison. The test model had a total length 35.1 cm, which is equivalent to six calibers. One caliber is equivalent to one diameter of the cylinder part of the body specified as 5.715 cm. The nose geometry was modeled as a 3-caliber-long secant-ogive, and the cylinder section was 3 caliber long. The radius of the secant-ogive was 1079 mm. The incidence angle was 10 deg. The TLNS and the matching of PNS and TLNS results were compared with the experiment.[18] The matching position is at $x/D = 0.5$. In most of the cases, the accuracy of PNS–TLNS matching was near to the TLNS result. Because of the limitation of computer resources for TLNS code, streamwise distance of generated grid points was very large in comparison to vertical and circumferential distance of grid points. In the PNS code one can choose a very small streamwise grid size. In spite of this fact, the accuracy of the results usually is less than that of TLNS results. This is because of the existence of flow separation at $x/D > 3$, which decreases the accuracy of results in the leeward region for PNS code. Because of a high incidence angle and a large viscous layer at the leeward of the ogive, the accuracy of the results is less than in comparison to incidence angle of 6 deg. (It is not shown here because of space limitation.) It is notable that in the final stage of the ogive the accuracy of the TLNS is much better than of the matching of the PNS and TLNS. Decrease on the accuracy of PNS results is caused by the large separated viscous layer at leeward.

Now, we investigate the effect of position of initial data plane on the accuracy of PNS code. Figure 3 shows this comparison. The interface plane for the case 1 is at the $x/d = 0.5$ and for the case 2 is at $x/d = 3.5$, and it is notable that the results are the same, except on the windward. In other words, the position of the generated initial data plane by TLNS code does not affect certainly on the accuracy of the PNS code in the final stages of the ogive. Even the result of the first case is better than the second at the windward. It can be justified by some of the errors that are at the starting plane of a PNS code. At the second case the starting plane is near to the comparison location.

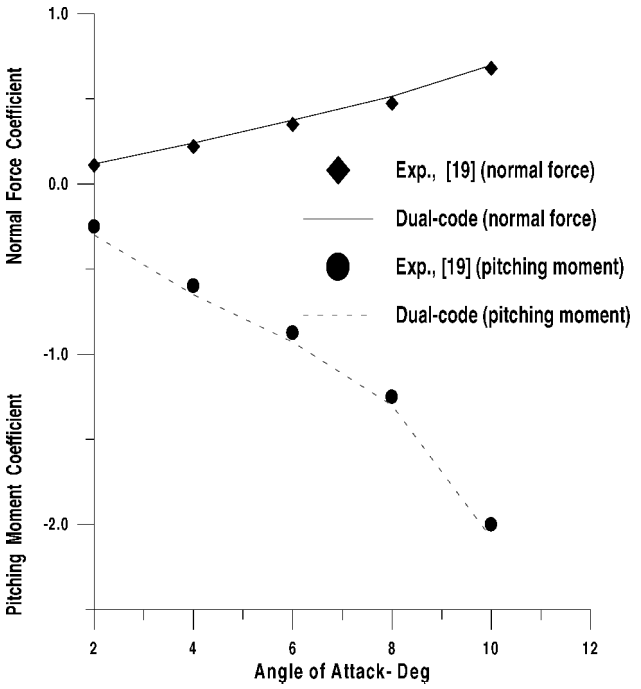

Fig. 4 Normal-force and pitching-moment coefficients: Mach number = 3 and spin rate = 0.19.

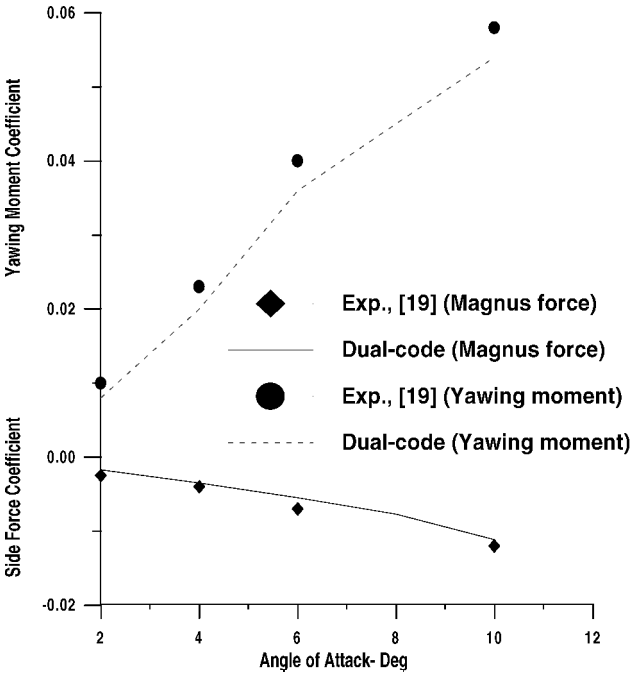

Fig. 5 Side-force (Magnus) and yawing-moment coefficient: Mach number = 3 and spin rate = 0.19.

In this section the results of the computation of the magnus effect are considered. The model configuration is the same as the first case, and the experimental data are extracted from Neitubicz et al.[19] The dimensions of the computational grid used for TLNS code at the nose of the ogive are $6 \times 48 \times 82$ in the longitudinal, radial, and circumferential directions. The dimensions of the computational grid for the PNS code at the afterbody of the ogive-cylinder are 57×102 in the radial and circumferential directions. The grid-convergence test showed that the mentioned grid size is enough.

In Fig. 4 normal-force and pitching-moment coefficients at different angles of attacks are shown. The nondimensional spin rate of the ogive-cylinder is 0.19. The comparison with the experimental data shows acceptable accuracy.

The side-force (Magnus force) and yawing-moment coefficient are shown in Fig. 5. Comparison of the simulation results with the experimental data shows reasonable accuracy. Goshtasbi Rad[17] reported a more accurate result for angle of attack of 6 deg, but some adjustment of the turbulence model coefficient was needed.

As an example, the running time for one of the preceding cases is mentioned in the following. The CPU time for the full TLNS code with a grid size of $21 \times 48 \times 61$ was 38 h using a Pentium 4 (2 GHz), but the CPU time for a dual–code strategy with a crossflow grid size of 48×61 and a streamwise step size ($\Delta x/D$) equal to 0.0001 was 3 h.

Conclusions

One limitation of using the Navier–Stokes code for computation of the complex compressible flowfields is the requirement of extensive computer resources. In this study it is shown that using the dual-code strategy it is possible to significantly reduce the needed computer time. It is found that the required computer time for the dual-code approach is an order of magnitude less than that of the TLNS code. The results also show that the model predictions are in reasonable agreement with the experimental data. The capability of running this dual-code strategy on microcomputers could make the approach a useful tool for preliminary designs of spin-stabilized missiles.

Acknowledgment

The authors thank Goshtasbi Rad for making his PNS code available for use in this study.

References

[1]Edge, H., Sahu, J., Sturek, W., and Behr, M., "CFD Computations with ZNSflow CHSSI Software," Dept. of Defence High Performance Computing User Group Conf., June 1999.

[2]Behr, M., Pressel, D. M., and Sturek, W. B., "Comments on CFD Code Performance on Scalable Architectures," *Computer Methods in Applied Mechanics and Engineering*, Vol. 190, No. 3–4, 2000, pp. 263–277.

[3]Anderson, D. A., Tannehill, J. C., and Pletcher, R. H., *Computational Fluid Mechanics and Heat Transfer*, 1st ed., Hemisphere, New York, 1984, pp. 420–433.

[4]Wood, W. A., Thompson, R. A., and Eberhardt, S., "Dual Code Solution Strategy for Hypersonic Flows," *Journal of Spacecraft and Rockets*, Vol. 33, No. 3, 1996, pp. 449–451.

[5]Gnoffo, P. A., "Code Calibration Program in Support of the Aero Assist Flight Experiment," *Journal of Spacecraft and Rockets*, Vol. 27, No. 2, 1990, pp. 131–142.

[6]Lawrence, S. L., Tannehill, J. C., and Chaussee, D. S., "Upwind Algorithm Parabolized Navier–Stokes Equations," *AIAA Journal*, Vol. 27, No. 8, 1993, pp. 1175–1183.

[7]Lawrence, S. L., Chaussee, D. S., and Tannehill, J. C., "Application of an Upwind Algorithm to the Three Dimensional Parabolized Navier–Stokes Equations," AIAA Paper 87-1112, June 1987.

[8]Tannehill, J., Buelow, P., Ievalts, J., and Lawrence, S., "A Three-Dimensional Upwind Parabolized Navier–Stokes Code for Real Gas Flows," AIAA Paper 89-1651, June 1989.

[9]Sturek, W. B., Guidos, B., and Nietubicz, C. J., "Navier–Stokes Computational Study of the Magnus Effect on Shell Bluntness at Supersonic Speeds," AIAA Paper 82-1341, 1982.

[10]Emdad, H., Alishahi, M. M., and Goshtasbi Rad, E., "Computation of High Reynolds Number Parabolized Navier–Stokes Equations Based on Upwinding Algorithm," *Scientia Iranica*, Vol. 6, No. 2, 1999, pp. 122–130.

[11]Roe, P. L., "Approximate Riemann Solvers, Parameter Vectors and Difference Schemes," *Journal of Computational Physics*, Vol. 43, 1983, pp. 357–372.

[12]Baldwin, B. S., and Lomax, H., "Thin Layer Approximation and Algebraic Model for Separated Turbulent Flows," AIAA Paper 78-257, Jan. 1978.

[13]Alishahi, M. M., Emdad, E., and Abouali, O., "3-D Thin Layer Navier–Stokes Solution of Supersonic Turbulent Flow," *Scientia Iranica*, Vol. 10, No. 1, 2003, pp. 74–83.

[14]Alishahi, M. M., Emdad, E., and Abouali, O., "3-D Thin Layer Navier–Stokes Solution of Supersonic Laminar Flow," *Proceeding of 5th International and 9th Annual Mechanical Engineering Conference of Iran*, ISME, 2001, pp. 285–299.

[15]Chackravarthy, S. R., and Szema, K. Y., "Euler Solver for Three-Dimensional Supersonic Flows with Subsonic Packets," *Journal of Aircraft*, Vol. 24, No. 2, 1987, pp. 73–83.

[16]Alishahi, M. M., Emdad, H., and Abouali, O., "3-D Solution of Euler Equations for Supersonic Flow with Roe's Method," *Proceedings of AERO 2000*, Vol. 1, Iranian Aerospace Society, Tehran, Iran, pp. 181–190.

[17]Goshtasbi Rad, E., "Navier–Stokes Solutions of the Spinning Bodies at Supersonic Speeds," Ph.D. Dissertation, Shiraz Univ., Shiraz, Iran, May 1999.

[18]Raklis, R. P., and Sturek, W. B., "Surface Pressure Measurements on Slender Bodies at Angle of Attack at Supersonic Speeds," U.S. Army Ballistic Research Lab., ARBRL-MR-02876, Aberdeen Proving Ground, MD, Nov. 1978 (AD A064097).

[19]Neitubicz, C. H., and Opalka, K. O., "Supersonic Wind Tunnel Measurements of Static and Magnus Aerodynamic Coefficients for Projectile Shapes with Tangent and Secant Ogive Noses," U.S. Army Ballistic Research Lab., ARBRL-MR-02876, Aberdeen Proving Ground, MD, Feb. 1980 (AD A083297).

R. M. Cummings
Associate Editor